Supplementary information

Non-adiabatic origin of Roaming OH in the formic acid dimer dication

Saroj Barik[1¶], Ester Livshits[1,2¶], Roi Baer[1,2*] and Daniel Strasser[1*]

[1] Institute of Chemistry, The Hebrew University of Jerusalem, Jerusalem 9190401, Israel

[2]Fritz Haber Research Center for Molecular Dynamics, The Hebrew University of Jerusalem, Jerusalem 9190401, Israel

* emails: strasser@huji.ac.il, roi.baer@huji.ac.il

¶ These authors contributed equally to this work

Supporting information includes the following chapters:

- Measured product branching ratios in the formic acid dimer dication breakup
- Measured yields as a function of EUV pump – near-IR probe delay
- Typical roaming OH trajectory simulation, forming a neutral OH product
- Typical H_2O^+ forming trajectory, initiated on the S2 state
- Simulated trajectory ensemble
- Mulliken Charge and Excited-State Energetics Analyses of FA_2^{2+} states
- The effect of one FA^+ monomer on the dissociation of the second FA^+

Measured product branching ratios in the formic acid dimer dication breakup

Ion coincidence measurements allow identifying all the product channels of the FA_2^{2+} breakup shown in Figure S1. Only one two-body breakup channel is attributed to formic acid dimer ionization, the $FA^+ + FA^+$. Strict momentum conservation requirements were applied to the measured coincidences, allowing disentangling true coincidences from random coincidences of singly ionized monomers. The branching ratios of the two-body, three-body and four-body breakup channels are shown in figure S1, for clarity, channels with <1% branching ratios are omitted from the figure. The channels are identified by the measured pair of ion masses and the missing neutral mass is attributed to neutral H, H_2, OH and CO products. The branching ratios are corrected for random coincidence background and for channel dependent detection efficiencies, which are estimated by assuming cylindrically symmetric fragmentation around the laser polarization axis. Within the experimental error, we observed no significant evidence for scrambling of the two FA monomers, supporting the theoretical modeling of the one of the dimers as a point charge object. In both three- and four-body breakup, the predominant channel exhibits ejection of a neutral OH product.

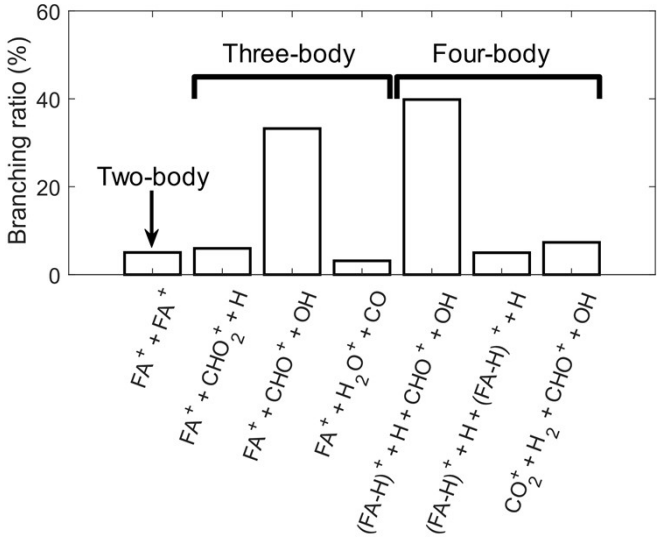

Figure S1 *measured branching ratio of FA_2^{2+} product channels produced by single photon double ionisation of FA_2.*

Measured yields as a function of EUV pump – near-IR probe delay

Figure S2a shows the two-body product channel yield, measured as a function of the near-IR delay time. The red bars indicate the average yields at positive versus negative time delays, indicating a substantial ~20 ± 3% suppression of the $FA^+ + FA^+$ yield when the near-IR pulse arrives after the ionizing EUV pulse. In contrast, figure S2b shows the combined yields of the two predominant channels that exhibit OH formation. Both channels exhibit ~ 7 ± 1% enhancement when the near-IR pulse arrives after the ionizing EUV. The observed behavior is consistent with the theoretical simulation of predominant two-body breakup on the dication ground-ground state that may be suppressed by excitation to the higher lying states which predominantly contribute to the three-body breakup. Nevertheless, one can note that the absolute suppression of the less abundant $FA^+ + FA^+$ yield can only account for up to ~2% enhancement of the combined yield of the predominant channels. As the $FA^+ + H_2O^+ + CO$ channel also originated from higher lying state, it is expect that the yield of this channel will also enhance with positive near-IR probe delay, however within the finite statistics it is difficult to observe as shown in figure S2c.

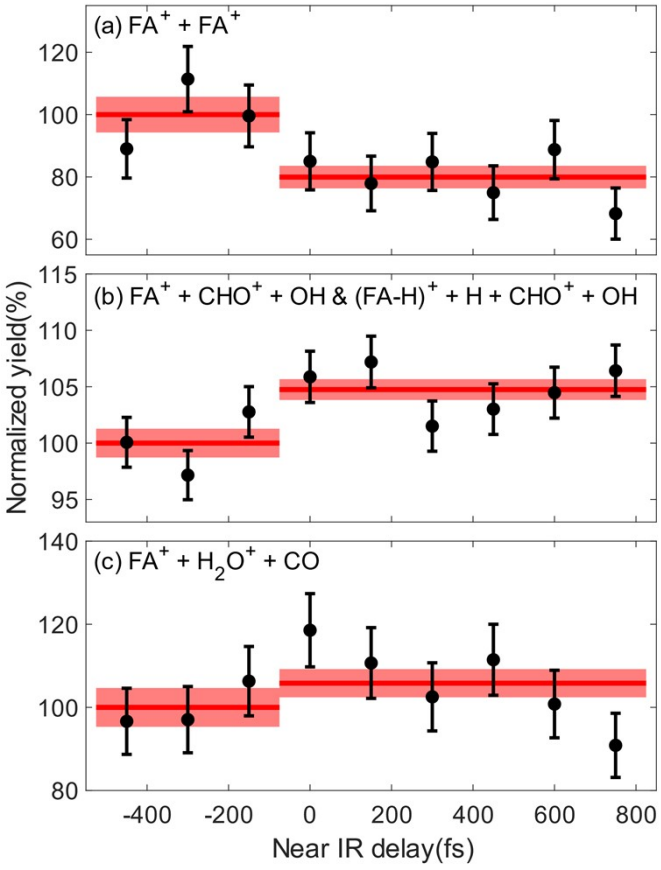

Figure S2 *shows the measured yield as a function of near-IR probe delay. The $FA^+ + FA^+$ channel shows 20% suppression while the $FA^+ + CHO^+ + OH$ and $(FA\text{-}H)^+ + H + CHO^+ + OH$ channels together show 7% enhancement in the positive time of near IR delays. The bottom panel shows the $FA^+ + H_2O^+ + CO$ channel where the yield remains same in both negative and positive near IR probe delay.*

Typical roaming OH trajectory simulation, forming a neutral OH product

Figure 2 of the main text shows a typical roaming OH trajectory simulation, culminating in proton-transfer and formation of an H_2O^+ product. Here, figure S3 shows a competing roaming OH trajectory on the S1 potential that results in ejection of the roaming OH. The black dash curve in the top panel shows the evolution of C-C distance after double ionization of FA_2. The C-C distance increases rapidly due to the Coulomb repulsion. The color-coded curve represents the H-OH distance evolution in the dissociating FA^+ after double ionization of FA_2, where the color encodes the electronic potential at different times, indicating that at ~40fs the FA_2^{2+} exhibits a non-adiabatic transition from S1 to S0. The bottom panel shows the time evolution of FA_2^{2+} potentials showing that the non-adiabatic transition occurred at a conical intersection of the two states. Following the transition to S1, the H-OH distance increases and roaming OH motion begins until at ~445 fs the H-OH distance increases beyond ~3.6 Å and never comes back. The shaded region indicates the roaming OH duration. The H-OH distance oscillates a couple of times until the neutral OH is eventually ejected. Note that the splitting of the first excited state and ground-state vanishes when the OH radical is sufficiently separated from the ionic charge. Thus, although the final state is the first excited state, indicated by the red color-coded electronic state, the roaming system is mostly in a doubly degenerate ground-state.

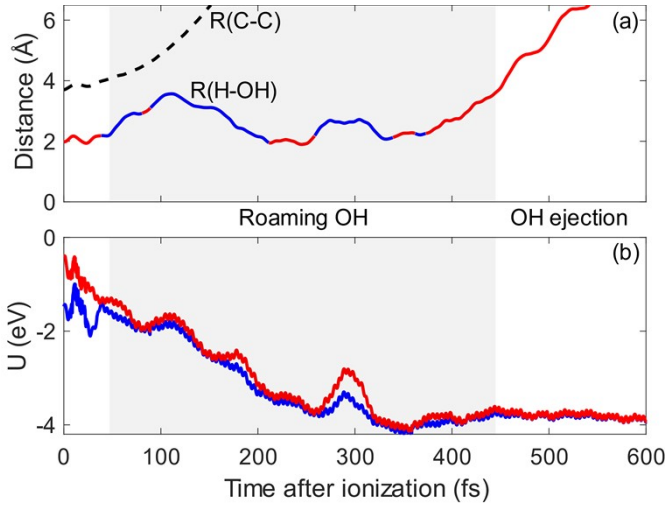

Figure S3 shows a typical simulated dynamics initiated on the S1 potential surface and exhibiting roaming OH, followed by ejection of the neutral radical. Top panel shows the evolution of C-C and H–OH distances and bottom panel shows the evolution of FA_2^{2+} potentials as a function of time after double-ionization.

Typical H_2O^+ forming trajectory, initiated on the S2 state

Figure S4 shows a typical roaming OH trajectory, initiated on the S2 state of FA_2^{2+}. Here, the roaming OH commences after the system undergoes two non-adiabatic transitions, from the S2 to S1 and then from S1 to S0. Similar to the typical trajectory initiated on the S1 state (shown in figure 2 of the main text), the roaming OH and the following proton-capture that forms H_2O^+ proceed on the S0 ground-state.

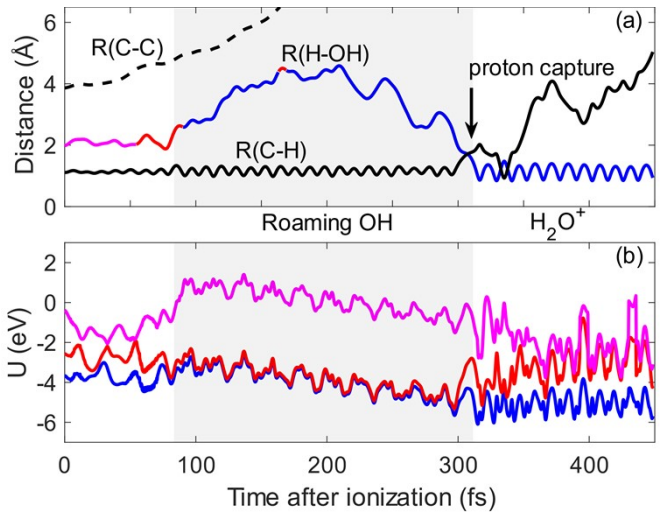

Figure S4 shows a typical H_2O^+ forming trajectory, initiated on the S2 state. Panel (a) shows the evolution of C-C, C-H and H – OH distance after double ionisation of FA_2 where the OH roaming dynamics is visible from C-H and H-OH curves. Pannel (b) shows the time evolution of S0, S1 and S2 potentials, showing conical intersections at ~53fs when the system hops from the S2 to the S1 potential, and at ~90 fs, when the system transitions to the S0 ground-state and roaming OH commences.

Simulated trajectory ensemble

A total of 100 trajectories were simulated on each FA_2^{2+} potential surface. The roaming OH trajectories, shown above as well as in the main text, show the typical roaming OH dynamics culminating in OH radical or H_2O^+ formation, initiated on the excited S1 and S2 states. Nevertheless, while the initial steps of charge separation and the non-adiabatic transition to the ground state are similar, the trajectory ensemble exhibits a broad distribution of roaming OH times, as shown in Figure S5. Figure S5a shows the OH ejection time for the $FA^+ + CHO^+ + OH$ channel. The empty red and full magenta bars represent the yields from the S1and S2 states, respectively. As discussed in the main text, the OH ejection initiated from the S1 state takes longer, up to 1ps times, compared with dynamics initiated on the higher lying S2 state, for which most trajectories exhibit OH release before 200 fs. In contrast, roaming OH trajectories that culminate in proton transfer and the formation of H_2O^+ exhibit a broad distribution, with long roaming times for trajectories initiated on both the S1 and S2 states. Figure S5c shows the secondary dissociation times for the rare (3) simulated events that exhibit ejection of a neutral H atom, resulting in the $FA^+ + (FA\text{-}H)^+ + H$ product channel, which were all initiated on the S2 state potential.

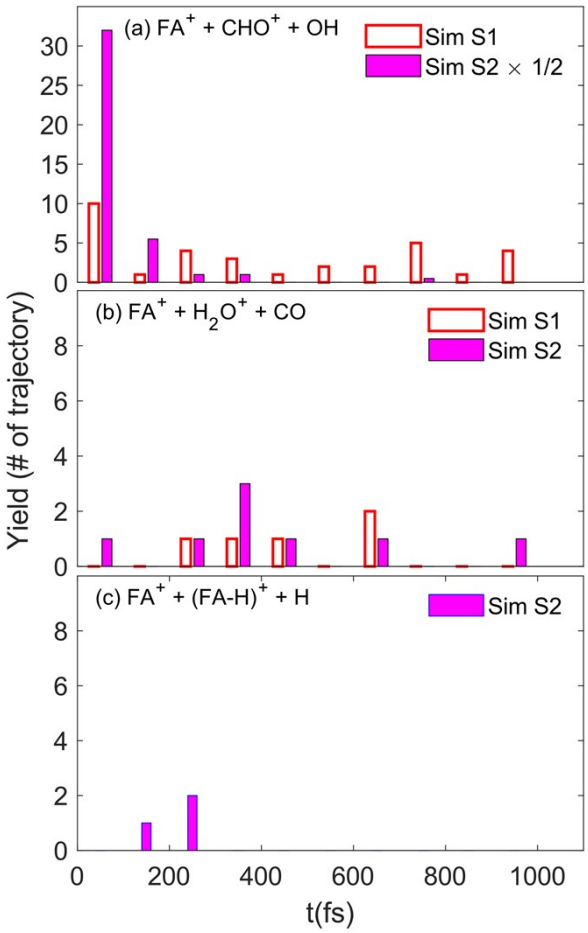

Figure S5 Secondary dissociation times of the simulated trajectory ensemble response. Empty red bars indicate trajectories initiated on the S1 state, while full magenta bars indicate trajectories initiated on the S2 state. The distributions are resolved according to the final product channel: (a) $FA^+ + CHO^+ + OH$, (b) $FA^+ + H_2O^+ + CO$, and (c) $FA^+ + (FA\text{-}H)^+ + H$.

Mulliken Charge and Excited-State Energetics Analyses of FA^{2+}_2 states

Here, we present the singlet and triplet energetics and Mulliken charge analyses of the ground and excited states of the FA dication dimer, explicitly calculated with XMS-CASPT2(26e16o)/aug-cc-pvdz at the Franck-Condon geometry (shown in Table 1). The explicit calculations of the entire dimer are compared with the model using a point charge to describe one of the monomers and with a more economic calculation with XMS-CASPT2(13e9o)/aug-cc-pvdz that makes the NA-AIMD dynamics simulations feasible.

Table 1. FC geometry used for the Mulliken charge analysis in Å.

	x	y	z
C	-1.848329	-0.146095	0.000000
O	-1.146508	-1.134677	0.000000
O	-1.429690	1.070058	0.000000
H	-0.410078	1.118739	0.000000
H	-2.947369	-0.227301	0.000000
C	1.848326	0.146091	0.000000
O	1.146524	1.134687	0.000000
O	1.429678	-1.070059	0.000000
H	0.410059	-1.118761	0.000000
H	2.947369	0.227280	0.000000

Singlet states

Table 2 summarizes the Mulliken charge distribution and electronic energies of the FA^{2+}_2 singlet in its ground state (GS) and two excited states (1ex and 2ex). The bottom part of the first section lists the total electronic energies (in a.u.) and corresponding excitation energies (in eV), showing that the first and second excited states lie 0.70 eV and 0.74 eV above the ground state, respectively. For each state, Mulliken charges are provided for all atoms in the two monomers (C, O, O, H, H for each monomer). Each monomer is indicated by green or yellow color. The data reveal modest but systematic charge redistribution upon excitation: a slight transfer of electron-density from the OH to the HCO moiety on one of the monomers for state 1 and the other for state 2, resulting in similar ~0.7 eV increase in the corresponding excitation energies.

Table 2. Mulliken charge distribution of FA_2^{2+} *in the singlet ground and excited states. The last three columns give the total charge per monomer, and the lower part of the table lists the total electronic energies (in a.u.) and the corresponding excitation energies (in eV).*

		Mulliken charge distribution			**Charge per monomer**		
		GS	1ex	2ex	GS	1ex	2ex
Monomer 1	C	0.885	0.875	0.859	1.006	0.988	1.014
	O	-0.118	-0.161	-0.193			
	O	-0.188	-0.159	-0.081			
	H	0.367	0.392	0.414			
	H	0.059	0.042	0.015			
Monomer 2	C	0.902	0.865	0.885	0.994	1.012	0.986
	O	-0.118	-0.202	-0.165			
	O	-0.175	-0.044	-0.126			
	H	0.328	0.380	0.357			
	H	0.058	0.014	0.035			
Molecule	E(a.u)	-377.642	-377.616	-377.615			
	ΔE(eV)	0.000	0.70	0.74			

The last three columns present the total charge per monomer for GS, 1ex, and 2ex. These values remain close to +1 for each monomer across all electronic states. The data clearly show pronounced charge separation between the two monomers: each monomer carries approximately +1 charge, consistent with the dimer's overall +2 charge. Within each monomer, the carbon atom bears the dominant positive charge. The distance between the carbon atoms is about 3.7 Å. This pattern persists across all electronic states and reflects the intrinsic polarity of the FA^+ fragment.

Triplet states

Table 3 shows the Mulliken charge distributions and excited state energies of the triplet dication states at the Franck–Condon dimer geometry. The similar behavior of the triplet and singlet states indicates that there's little interaction between the two doublet monomers, supporting the modeling of the dication dimer described in the main text.

Table 3. Mulliken charge distribution of FA_2^{2+} *in the triplet ground and excited states. The last three columns give the total charge per monomer, and the lower part of the table lists the total electronic energies (in a.u.) and the corresponding excitation energies (in eV).*

		Mulliken charge distribution			**Charge per monomer**		
		GS	1ex	2ex	GS	1ex	2ex
Monomer 1	C	0.905	0.874	0.895	0.999	1.024	0.977
	O	-0.101	-0.190	-0.130			
	O	-0.159	-0.019	-0.143			
	H	0.335	0.390	0.352			
	H	0.018	-0.031	0.003			
Monomer 2	C	0.905	0.895	0.884	1.001	0.976	1.023
	O	-0.100	-0.130	-0.185			
	O	-0.158	-0.143	-0.032			
	H	0.334	0.350	0.387			
	H	0.019	0.003	-0.031			
Molecule	E(a.u)	-377.642	-377.617	-377.616			
	ΔE(eV)	0.000	0.67	0.71			

Model system of a point charge and an explicit FA^+ monomer.

Here, we present the electronic energetics and Mulliken charge analysis of the formic acid cation (FA^+) monomer, while the second monomer is modeled as a movable point mass and point charge positioned at the location of its central carbon atom.

Table 4 summarizes the Mulliken charge distribution and electronic energies of the model system in its ground state (GS) and two excited states (1ex and 2ex). The lower part of the table reports the total electronic energies (in a.u.) and corresponding excitation energies (in eV). The higher 1.19 eV excitation energy of the 1ex, compared with the ~0.7 eV in the explicit higher-level modeling of the dimer, can be attributed to the effect of the neglected intermolecular hydrogen bonds. In this symmetry-broken model, only one of the monomers can be excited therefore the 2nd excited state at ~0.7 eV is not observed and the 3.35 eV excitation of the 2ex state of the model is attributed to a higher lying state that is not captured in the explicit modeling of the entire dimer.

Table 4. Mulliken charge distribution and total electronic energies of the formic acid cation (FA^+) monomer in the ground state (GS) and the first (1ex) and second (2ex) excited states. the lower part of the table lists the total electronic energies (in a.u.) and the corresponding excitation energies (in eV).

Mulliken charge distribution			
	GS	1ex	2ex
C	0.950	0.912	0.965
O	-0.157	-0.213	-0.042
O	-0.041	-0.057	-0.177
H	0.213	0.270	0.174
H	0.035	0.088	0.081
E(a.u)	-188.751	-188.708	-188.628
ΔE(eV)	0.00	1.19	3.35

The effect of one FA^+ monomer on the dissociation of the second FA^+

To evaluate the effect of one FA^+ monomer on the dynamics of the other monomer, we performed simulations of a single FA^+ monomer without the presence of the second monomer that was represented by a point charge in our model. Trajectories were initiated on the S1 and S2 states with the same initial conditions of the FA^+ monomer that were sampled in the dimer simulations. It is not possible to perform direct comparison of the KER distributions and three-body momentum correlations, as the monomer simulation can only consider the secondary dissociation event. Nevertheless, similar to the dimer dication dynamics, we observed that excited FA^+ monomer simulations can exhibit similar roaming OH dynamics and result in either OH or H_2O^+ products. However, several differences can be clearly noted. As stated in the main text, when the second FA^+ effect is considered by including a point charge, only 16% of the trajectories initiated on the S1 state contribute to the two-body $FA^+ + FA^+$ channel. In contrast, 64% of the simulated FA^+ monomer trajectories on the S1 state exhibit a stable monomer with no indication of roaming-like dynamics within 1ps. Another difference that can be reported concerns the time (after ionization) at which nonadiabatic hopping occurs from the S1 state to the ground state. Figure S6 shows that the dimer model S1→S0 transition times can be described by a 57 ± 4 fs lifetime. Monomer simulations exhibit a twice longer 117 ± 12 fs lifetime. Furthermore, in both S1 and S2 FA^+ monomer simulations H_2O^+ formation was at least twice less likely compared with the simulated dimer dynamics. We can conclude that while roaming OH dynamics are not unique to the dimer dication, the charge of the nearby monomer affects the early-stage dynamics that in turn can affect the final product branching ratios.

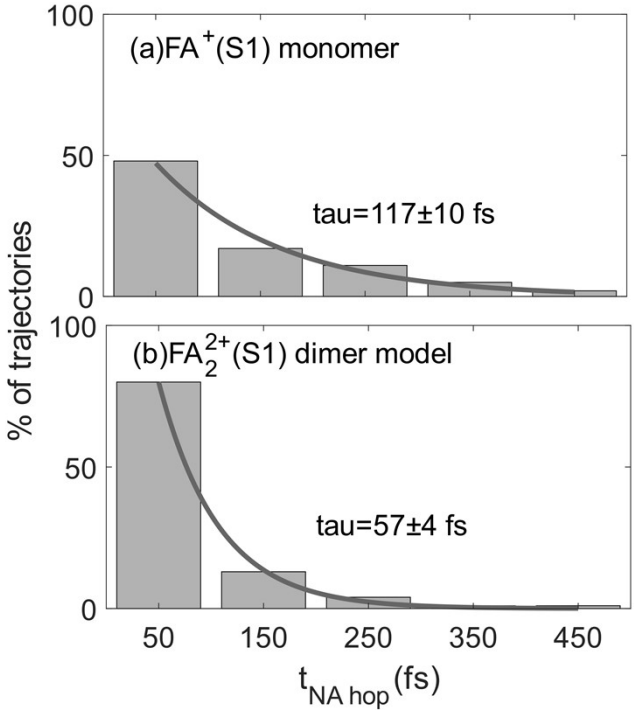

Figure S6 Simulated nonadiabatic S1→S0 hopping times distributions, fitted with an exponential decay lifetime. (a) FA^+ monomer simulations (b) FA_2^{2+} dimer simulations, considering one of the monomers as a point charge.